Co-Pyrolysis Behavior, Kinetic and Mechanism of Waste-Printed Circuit Board with Biomass

Prajapati , Sonalben B; Gautam , Alok ; Gautam , Shina ; Yao , Zhitong ; Tesfaye, Fiseha; Lü , Xiaoshu

Published in:
Processes

DOI:
10.3390/pr11010229

Published: 10/01/2023

Document Version
Final published version

Document License
CC BY

processes

MDPI

Article

Co-Pyrolysis Behavior, Kinetic and Mechanism of Waste-Printed Circuit Board with Biomass

Sonalben B. Prajapati [1,2], Alok Gautam [2,3,*], Shina Gautam [2,3,*], Zhitong Francisco Yao [4], Fiseha Tesfaye [5,*] and Xiaoshu Lü [6]

1 Chemical Engineering Department, Government Engineering College, Bhuj 370001, India
2 Department of Chemical Engineering, Gujarat Technological University, Chandkheda, Ahmedabad 382424, India
3 Chemical Engineering Department, Shroff S. R. Rotary Institute of Chemical Technology, UPL University of Sustainable Technology, Bharuch 393135, India
4 College of Materials and Environmental Engineering, Hangzhou Dianzi University, Hangzhou 310018, China
5 Johan Gadolin Process Chemistry Centre, Åbo Akademi University, Henrikinkatu 2, FI-20500 Turku, Finland
6 Department of Electrical Engineering and Energy Technology, University of Vaasa, FI-65200 Vaasa, Finland
* Correspondence: alokgautam2002@gmail.com (A.G.); shinaiitd@gmail.com (S.G.); fiseha.tesfaye@abo.fi (F.T.)

Abstract: Waste-printed circuit boards (WPCBs) account for approximately 3–6 wt% of total electronic waste. Due to their content of thermosetting materials and added brominated fire retardants, their recycling and disposal is difficult and not eco-friendly. Pyrolysis as a thermal degradation process may assist in the solution of this problem. In addition, using biomass as an additive can upgrade the bio-oil and fix bromines in the char. In this study, cotton stalk (CS) is chosen as an additive and kinetic of the pyrolysis of three samples namely: PCB, CS, and CS:PCB (50:50) were investigated by the thermogravimetric analyzer (TGA) at heating rates of 5, 10, and 15 K/min. Three non-isothermal methods: FWO, KAS, and Starink were found in good agreement with the TGA data; however, the FWO method was more efficient in the description of the degradation mechanism of solid-state reactions. For CS and CS:PCB (50:50), α was increased from 0.2 to 0.9 with the FWO method, and calculated E_α values were found in the range of 121.43–151.88 and 151.60–105.67 kJ/mol in zone 1, while 197.06–79.22 and 115.90–275.06 kJ/mol in zone 2, respectively. Whereas, for PCB in zone 1, E_α values were found to be in the range of 190.23–93.88 kJ/mol. The possible decomposition mechanism was determined by the Criado method, which was in agreement with the mechanism model for reaction order $n = 3$. The oil product was also analyzed using Fourier-Transform Infrared Spectroscopy analysis.

Keywords: waste printed circuit board; electronic waste; cotton stalk; co-pyrolysis; kinetics

Citation: Prajapati, S.B.; Gautam, A.; Gautam, S.; Yao, Z.F.; Tesfaye, F.; Lü, X. Co-Pyrolysis Behavior, Kinetic and Mechanism of Waste-Printed Circuit Board with Biomass. *Processes* **2023**, *11*, 229. https://doi.org/10.3390/pr11010229

Academic Editor: Song Hu

Received: 28 November 2022
Revised: 28 December 2022
Accepted: 4 January 2023
Published: 10 January 2023

1. Introduction

The globe is facing a number of environmental issues because of increasing manufacturing activities. Due to the recent increase in the manufacturing of electronic devices and their ever-shortening spans of life, today, electronic waste (e-waste) has emerged as one of the major environmental concerns [1]. Currently, rapidly emerging countries, such as India and China, are the primary contributors of e-waste [2]. According to Wang et al. [3], 20–50 million tons of e-waste are generated worldwide each year, which is growing at a rate of 3–5% annually [4]. India has been ranked as the first among the top five e-waste generators with an estimated yearly generation of 2 million tons [5]. Among these e-wastes, waste printed circuit boards (WPCBs) make up 3–6% of total e-waste and they are heterogeneous mixture of organic materials, glass fibers, and metals [6]. They normally contain 30% plastics (polyethylene, polypropylene, polyesters, PVC, epoxy resins, PTFE, and nylon), 30% ceramic (primarily silica or alumina with some amount of mica) [7], alkaline earth oxides, and barium titanate [8]. They also contain 40% metals, with copper accounting

for 10–27% of the total weight of WPCBs. Other metals found are gold, silver, iron, and palladium. Some toxic metals such as antimony, cadmium, lead, nickel, arsenic, mercury, and chromium can have major environmental consequences if not recycled carefully [7].

PCBs are mainly manufactured with resins containing fire flame retardants such as tetrabromobisphenol A (TBBPA) and polybrominated diphenyl ethers (PBDEs) [9]. To facilitate their recycling, many sophisticated methods have been developed and applied in China and India [10], which include mechanical dismantling, to separate plastics and metals, hydrometallurgical and pyrometallurgical facilities, and amalgamation to recover valuable metals [11]. However, the separation of plastics with brominated flame retardants is not applied. Hence, the incineration of WPCBs and resulting waste produces a high quantity of dioxins, furans, and HBr with brominated phenols as by-products [12,13]. The brominated chemicals, such as their chlorinated congeners, can be hazardous to human skin, liver, and digestive tract. A number of studies have been carried out about the toxicity and health risks concerning human exposure to TBBPA on recycling sites [10,14,15]. Therefore, environmentally acceptable disposal or recycling of WPCBs is a big challenge [12]. The dibenzodioxins generated were mostly contained in the char matrix; nevertheless, research has revealed that polybrominated dibenzodioxins/furans (PBDD/Fs) were released at ppb and ppm levels during the breakdown process [13,16]. By adopting more appropriate processing conditions during recycling, it is possible to minimize the amount to which they are generated.

Pyrolysis appears to be one of the most promising technologies, allowing large polymer chains to be broken down into lighter polymer compounds with smaller molecular weight. Thermal decomposition of WPCBs initiates at 250 °C and continues to 900 °C [17]. Abdou et al. [17] observed the degradation of WPCBs below 550 °C and the polymeric matrix was not completely removed. Although the reaction process is influenced by the chemical composition and residence time, it is critical to developing methods and procedures for obtaining pyrolysis products with low halogen yields and reducing harmful emissions as much as possible. If the pyrolysis products have low yields of halogens, they can be utilized appropriately [16]. Furthermore, simplicity and effectiveness are especially important in developing a technique to produce the ideal synthetic liquid fuel. Moreover, WPCBs include a relatively high content of ash, so its energy density (e.g., heating value) and thermolysis efficiency are low. Co-pyrolysis of biomass with WPBCs could be an alternative technology that improves these two criteria [18]. A high amount of hydrogen present in biomass may lead to dehalogenation and prevention of PBDD/Fs which promotes HBr/HCl fixation in char. Furthermore, the biomass has a higher H/C molar ratio which can act as a hydrogen donor to WPCBs [19]. Water, one of the most abundant components in biomass, is expected to act as a reactive agent, promoting further cracking of the WPCBs tar and the production of more volatile chemicals that improves pyrolysis oil yields [18,20]. Co-pyrolysis of biomass has been shown in several studies to boost oil yield and quality while maintaining the overall process. However, because of the various reactivities of biomass and e-waste, this process is relatively complex. Pyrolysis product yields and characteristics are influenced by the temperature and blend ratio of feedstock [18,21].

Generally, the knowledge of the pyrolysis kinetics of the main thermal decomposition process is critical to predicting the pyrolysis behavior of a material and helps to design a suitable reactor, as well as the mathematical modeling of the reactor for process optimization. Process parameters, heat and mass transport limits, physical and chemical properties of the sample, and systematic errors are all factors that might affect the kinetic parameters. The key procedural challenges are dehalogenation and avoidance of highly toxic emissions (especially PBDD/Fs). The aim of this study is to probe the pyrolysis behavior of WPCB, cotton stalk (CS), and its blend. Three model-free methods, such as Kissinger–Akahira–Sunose (KAS), Flynn–Wall–Ozawa (FWO), and Starink, were used to calculate apparent activation energy (E_α) and pre-exponential factor (A). Furthermore, with calculated E_α values, the possible decomposition mechanism was probed using the Criado method. There is

no single work in the published literature that focused on the co-pyrolysis of these residues. The comparison of the thermal decomposition of PCB, CS, and its blend can be the first expanding research effort to understand the synergistic behavior of the mixture.

2. Kinetic Modeling

The concept of the single-step, solid-state reactions can be represented by the Arrhenius equation. It means that the reactant molecules are in an endothermic equilibrium with the active molecules that are involved in the reaction.

$$\kappa(T) = Ae^{\left(-\frac{E}{RT}\right)} \tag{1}$$

where E is the activation energy (kJ mol^{-1}) and A is the pre-exponential factor (>1). R refers to the gas constant (kJ mol^{-1} K^{-1}). T represents the temperature in K and $\kappa(T)$ is a rate constant. The value of E was supposed to be a constant for single-step reactions and it is the energy needed to turn inactive molecules into active molecules. To describe the kinetic expression from the mass balance of a reacting solid and the conversion degrees for a single-phase reaction, the thermogravimetric results can be expressed as [22]:

$$\frac{d\alpha}{dt} = k(1-\alpha)^n \tag{2}$$

where n is reaction order. A general kinetic Equation (2) is based on assumption that the rate of process $d\alpha/dt$ is a function of two variables only: degree of conversion (α) and temperature (T). Assuming that the function of two variables can be substituted by a product of two functions variables, $\kappa(T)$ and $f(\alpha)$. Therefore, the rate of heterogeneous solid reactions can be described as [23]:

$$\frac{d\alpha}{dt} = \kappa(T)f(\alpha) \tag{3}$$

where $\kappa(T)$ and t are rate constant and time, respectively. α is the degree of conversion, ranging from 0 to 1. $f(\alpha)$ is the reaction model that represents a certain solid-state mechanism [24]. The degree of conversion can be defined as:

$$\alpha = \frac{m_0 - m_t}{m_0 - m_f} \tag{4}$$

where m_0, m_t, and m_f are the initial, instantaneous, and final mass of the sample. Integrating Equation (1) into Equation (3), the rate of a solid-state reaction can be expressed as:

$$\frac{d\alpha}{dt} = Ae^{-E/RT} f(\alpha) \tag{5}$$

where E, A, and reaction model $f(\alpha)$ are called kinetic triplets [23]. If the reaction is studied under non-isothermal conditions at a linear heating rate, $\beta = dT/dt$. In which Equation (5) becomes:

$$\frac{d\alpha}{dT} = \frac{A}{\beta} e^{-E/RT} f(\alpha) \tag{6}$$

Actual solid-state reaction is complex, which includes multiple solid–gaseous reactions with different rates, such as adsorption, desorption, sublimation of gaseous products or reactants on the surface of a reacting solid, and diffusion of gaseous products or reactants through a solid [24,25].

Therefore, the effective activation energy derived from the overall kinetic data is a composite number determined by the activation energies of the individual stages and their relative contributions to the overall reaction rate. As a result, the effective activation energy is usually a function of either temperature and conversion, or merely temperature. That is why the concept of variable activation energy E_α is more suitable to the non-elementary

nature of heterogeneous solid-state reactions. It should be used to explain how overall reaction rates are affected by temperature [26]. According to the previous studies, this obtained activation energy is the apparent one and does not have any mechanistic significance [27].

2.1. Model-Free Methods

There are two basic methods to calculate the kinetic triplets of complex solid-state reactions, namely model-fitting and model-free (or iso-conversion) methods. The model-fitting approaches use a single unpredictable heating rate [26], whereas the model-free method uses several heating rates, which eliminates mass transfer constraints. Dhaundiyal et al. [15] employed a model-fitting approach (Coats Redfern method [28]) to test the validity of the model-free method and produce the best appropriate reaction model for the decomposition of weed and lignocellulosic materials, respectively. They observed that kinetic parameters derived at various heating rates for models, differed significantly from those computed using the model-free method.

The force-fitting of non-isothermal data to a hypothetical reaction model is the initial cause of disagreement between model-free and model-based runs. Arrhenius parameters are calculated in the form of $g(\alpha)$ in the model fitting of Coats Redfern method, which is previously assumed and not able to discriminate separately temperature dependence of rate constant and conversion resulting in erroneous estimates of Arrhenius parameters.

The possibility of multi-reaction pathways is another key cause of disagreement, as the activation energy determined using the model-based method is a function of T and α. However, the calculated value of activation energy represents the average value for the overall process. It is derived in such a way that it is invariant with the reaction mechanism and kinetics that depend on the change in temperature and degree of conversion. With model-free methods, there is an opportunity for estimating the relative reactivity of solids by comparing the respective consumed time to accomplish the same extent of conversion at the same temperature. Therefore, these are called the iso-conversion method, and the parameters are calculated as a function of the conversion rate [25,27]. In other words, these methods used the rate data associated with a constant conversion to eliminate the reaction rate dependency on the conversion [27]. Therefore, iso-conversional approaches, as recommended by [27,29], are more realistic and exact when modelling non-isothermal pyrolytic kinetics.

By integrating Equation (6), replacing E/RT by x, and making rearranging Equation (7) can be written.

$$g(\alpha) = \frac{A}{\beta}\int_{To}^{Tmax} e^{(-\frac{E}{RT})}dT = \int_0^{\alpha}\frac{d\alpha}{f(\alpha)} = \frac{AE}{\beta R}p(x) \quad (7)$$

where $p(x)$ is a function known as the Arrhenius integral, which can be calculated numerically or by using various approximations. When we utilize Doyle's estimate [29,30] for $p(x)$, we get the popular equation proposed by Ozawa [31] for determining the activation energy by iso-conversion methods from Equation (3). Doyle [29,30] reported that for $20 < E/RT < 60$, $log_p\ (E/RT)$ may be closely approximated by Equation (8) [32]:

$$Log\ p\ (\frac{E}{RT}) \cong -2.315 - 0.457\ \frac{E}{RT} \quad (8)$$

That can be reduced to Flynn–Wall–Ozawa equation [33]:

$$ln\ \beta\ =\ ln\ \frac{AE_\alpha}{g(\alpha)R} - 5.330 - 1.052\ \frac{E_\alpha}{RT} \quad (9)$$

where E_α is the apparent activation energy or can also be called variable activation energy. The plot of $ln\ \beta$ against $1/T$ at different heating rates gives a straight line with the slope $-1.052\ E_\alpha/R$. Finding the slope for different (α) reveals the dependency of E_α on α [33].

Murray and White [34,35] provided a more precise estimate for $20 < E/RT < 50$ in the form of Kissinger, sometimes known as the Kissinger–Akahira–Sunose (KAS) equation [15,36].

$$ln\left(\frac{\beta}{T^2}\right) = ln\left(\frac{AE_\alpha}{Rg(\alpha)}\right) - \frac{E_\alpha}{RT} \quad (10)$$

For a constant value of α, plotting $ln\ (\beta/T^2)$ vs. $1/T$ will give a straight line with a slope of E_α/R. The profile of apparent activation energy can be generated for the different conversions [37]. Starink approximated the expression of FWO and KAS method, which can be transformed into the same general formula as [38]:

$$ln\left(\frac{\beta}{T^S}\right) = C - \left(B\frac{E_\alpha}{RT}\right) \quad (11)$$

where $s = 0$ and $B = 0.4567$ for FWO method, and $s = 2$ and $B = 1$ for KAS method. According to Starink, both parameters can be adjusted to $s = 1.8$ and $B = 1.0033$. As a result, the Starink equation can be rewritten as [30,31]:

$$ln\left(\frac{\beta}{T^{1.8}}\right) = C - 1.0037\left(\frac{E_\alpha}{RT}\right) \quad (12)$$

where $C = ln\left(\frac{AE_\alpha}{Rg(\alpha)}\right)$, for a given conversion fraction α, the points of $ln\ (\beta/T^{1.8})$ versus $1/T$ at different heating rates can be fitted to a straight line and the slope of the line corresponds to $1.0037\left(\frac{E_\alpha}{RT}\right)$. As a result, the slope of the straight line can be used to estimate the value of E_α.

2.2. Criado Method

Many studies that have examined experimental data for the solid-state mechanism have used reference theoretical curves, referred to as "master plots" in their analyses [34]. It uses the concept of reduced time plots, introduced by Ozawa [24,34] for α against $t/t\alpha$, where t_α is the time to reach a certain value of α (usually 0.5 to 0.9). In this sense, the master plot is a characteristic curve independent of the measurement condition, which is readily obtained from experimental results [39].

To use this method for the determination of the reaction mechanism, the known value of E_α is required [40]. For that, experimental data can be compared against a collection of theoretical model plots and the model that exactly matches the data can be chosen. This makes it possible to view the data in terms of the mechanism described by the chosen reaction model. The master theoretical curves can be generated through the $Z(\alpha)$ function [39,40]:

$$Z(\alpha) = f(\alpha)\ g(\alpha) \quad (13)$$

$Z(\alpha)$ versus α for different reaction mechanisms can be plotted as presented in Table 1 [29,31,36,40]. The equation is given by:

Theoretical curve:

$$\frac{Z(\alpha)}{Z(0.5)} = \frac{f(\alpha)g(\alpha)}{f(0.5)g(0.5)} \quad (14)$$

Experimental curve:

$$\frac{Z(\alpha)}{Z(0.5)} = \left(\frac{T_\alpha}{T_{0.5}}\right)^2 \frac{(d\alpha|dt)_\alpha}{(d\alpha|dt)_{0.5}} \quad (15)$$

By plotting $\frac{Z(\alpha)}{Z(0.5)}$ *vs* α for different mechanisms, a theoretical curve will be obtained. By the derived apparent activation energy plot, the experimental curve can be made. By comparing the two curves, the most reliable reaction mechanism can be found.

Table 1. Different degradation mechanisms with $f(\alpha)$ and $g(\alpha)$.

No.	Function Name	Mechanisms	$f(\alpha)$	$g(\alpha)$
m1	Jander equation	Diffusion, 3D (spherical symmetry)	$3/2(1-\alpha)^{2/3}[1-(1-\alpha)^{1/3}]^{-1}$	$[1-(1-\alpha)^{1/3}]^{1/2}$
m2	G–B equation	Diffusion, 3D (column symmetry)	$3/2[(1-\alpha)^{-1/3}-1]^{-1}$	$1-2\alpha/3-(1-\alpha)^{2/3}$
m3	Anti–Jander equation	Diffusion, 3D	$3/2(1+\alpha)^{2/3}[(1+\alpha)^{1/3}-1]^{-1}$	$[(1+\alpha)^{1/3}-1]^2$
m4	Z–L–T equation	Diffusion, 3D	$3/2(1-\alpha)^{4/3}[(1-\alpha)^{-1/3}-1]^{-1}$	$[(1-\alpha)^{-1/3}-1]^2$
m5	Avrami–Erofeev Equation	Random nucleation and nuclei growth, $n = 3$	$3(1-\alpha)\,[-\ln(1-\alpha)]^{2/3}$	$[-\ln(1-\alpha)]^{1/3}$
m6	Avrami–Erofeev Equation	Random nucleation and nuclei growth, $n = 2$	$2(1-\alpha)\,[-\ln(1-\alpha)]^{1/2}$	$[-\ln(1-\alpha)]^{1/2}$
m7	Avrami–Erofeev Equation	Random nucleation and nuclei growth, $n = 3/2$	$3/2(1-\alpha)\,[-\ln(1-\alpha)]^{1/3}$	$[-\ln(1-\alpha)]^{2/3}$
m8	Avrami–Erofeev Equation	Random nucleation and nuclei growth, $n = 4/3$	$4/3(1-\alpha)\,[-\ln(1-\alpha)]^{1/4}$	$[-\ln(1-\alpha)]^{3/4}$
m9	Geometrical contraction	Shrinkage geometric shape (column symmetry)	$3(1-\alpha)^{2/3}$	$1-(1-\alpha)^{1/3}$
m10	Geometrical contraction	Shrinkage geometric shape, (spherical symmetry)	$2(1-\alpha)^{1/2}$	$1-(1-\alpha)^{1/2}$
m11	Reaction order $n = 2$	Chemical reaction	$(1-\alpha)^2$	$(1-\alpha)^{-1}-1$
m12	Reaction order $n = 1$	Chemical reaction	$(1-\alpha)$	$-\ln(1-\alpha)$
m13	Reaction order $n = 3$	Chemical reaction	$(1-\alpha)^3$	$((1-\alpha)^{-2}-1)/2$

3. Materials

The CS sample was collected from a local farm in Gandhinagar, Gujarat, India. The samples were crushed and air-dried. The WPCBs sample was collected from Shivalik solid waste management, Punjab, India. The samples were ground and sieved before tests. The particle retained on 100 µm screen and passed from 210 µm screen were selected for the experiments for CS and WPCBs. During the mixing of WPCBs and CS samples, the partitioning method have been used to obtain a homogeneous representative sample. Table 2 shows the chemical compositions of the samples.

Table 2. Proximate and ultimate analysis of samples.

Sample	Calorific Value (Cal gm^{-1})	LOD (%)	Proximate Analysis			Ultimate Analysis			
			Ash (%)	Volatile Material (%)	Fixed C (%)	C (%)	H (%)	*n* (%)	S (%)
PCB	2788	14.05	43.95	41.87	0.13	26.73	2.39	1.93	0.19
CS	3411	23.93	5.49	70.51	0.07	32.52	4.12	2.15	0.16
CS:PCB (50:50)	3065	12	23.73	64.2	0.07	29.76	5.45	2.86	0.148

The heavy metal content was also evaluated using atomic absorption spectroscopy (AAS) and the results is displayed in Table 3. Copper is the most abundant metal in the printed circuit board, as expected from the literature [41].

Table 3. Heavy metal contents by AAS analysis in mg/L.

Sample	Cu	Zn	Ni	Cr	Mn	Pb	Fe
WPCBs	3937	25	22	4	44	18	1304

4. Experimental

Thermogravimetric analysis (TG-DTG) was performed using a Mettler Toledo analyser. The system was purged with 50 mL/min flow rate of N_2 gas. The drying step of TGA had a heating rate of 10 K/min for all three samples; whereas, the pyrolysis stages used three heating rates of 5, 10, and 15 K/min with approximately 10 mg of each sample. The

sample was placed in a ceramic crucible within the furnace and heated to 700 °C, after which the TG and DTG curves were calculated using an analytical computer system. The conventional furnace has a temperature precision of ±2 °C. The mass change of the sample with temperature during the heating process is recorded and the findings are utilized to compute the degradation kinetics. These experiments were repeated four times to be sure of the repeatability of the results. In addition, based on TGA findings, 200 mg of each sample pyrolyzed on lab-scale fixed bed equipment, using parameters such as 50 mL/min N_2 flow rate, 10 K/min heating rate, and ambient to 500 °C temperature variation. Finally, the generated liquid is collected and Fourier-Transform Infrared Spectroscopy (FTIR) analysis was made to identify the functional groups and bonds present in it.

5. Results and Discussion

5.1. Thermogravimetric Analysis

The thermogravimetric (TG), derivative thermogravimetric (DTG), and conversion curves for all three samples namely WPCBs, CS, and CS:WPCBs (50:50), at various heating rates are presented in Figures 1 and 2, respectively. Regardless of the varied heating speeds, both data show a similar trend of mass loss with temperature. However, with the increased heating rate the residual weight of the sample shifts to the right. The TG curve position, the maximum degradation rate, and the location of the highest peak temperature (T_m) are all affected by the heating rate. According to the DTG curves, when the heating rate increases, the active pyrolysis period's initial and ultimate temperatures increases as well. With an increased heating rate, the TG maximum points and DTG curve minimums move to higher temperatures, which can be explained by heat transfer limitations. At a low heating rate, the system receives more instantaneous thermal energy during the analysis, and it may take a long time for the purge gas to attain equilibrium with the furnace and sample temperature. While a faster heating rate reduces reaction time, the temperature required for the sample to breakdown is also higher.

There are three different areas as shown in TGA curves, Figures 1 and 2. The temperature zones appeared with a more or less prominent shoulder at nearly ambient to <180 °C, which shows approximately 1% weight loss for WPCBs due to the release of H_2O, CO_2, HBr, CH_4, and CH_3COCH_3. In the same temperature region, 10% weight loss of CS due to moisture loss associated with depolymerization and vitrification transition was observed, and 7% weight loss occurred for CS:PCB. This mass loss has also been attributed to physical changes, including softening and molecular rearrangement attributed to the emission of low molecular volatility gases prior to its decomposition. As can be seen from the plot, for different heating rate, the main pyrolysis process begins at about 180–207 °C, 147–173 °C, and 121–152 °C for WPCBs, CS, and CS:WPCBs, respectively. Then, it proceeds rapidly with increasing temperature until about 359–377 °C, 350–376 °C, and 341–366 °C for WPCBs, CS, and CS:WPCBs, respectively. According to Y kim et al. [13], in this stage between 250 and 350 °C, the fire retardant degrades, yielding brominated aromatics and HBr. Other researchers have also proved this phenomenon [42–45].

Furthermore, weight loss decreases slowly up to 577 °C for the second zone with different heating rates in the ranges 360–378 °C, 351–377 °C, and 442–466 °C for WPCBs, CS, and CS:WPCBs (50:50), respectively. At temperatures above 370 °C, the phenol resin degraded [44]; after that, devolatilization ceases indicating the char generation and carbonization stage, thus, obtaining carbon and ash as the final solid residues. Detailed information on debromination and generation of dioxines is discussed in our recent paper Prajapati et al. [40]. A residue of PCB at the end of the process is relatively very high (60 wt%) which is also in agreement with previous studies [12]. However, lower solid residues of 6% and 20% were found for CS and CS:WPCBs, respectively.

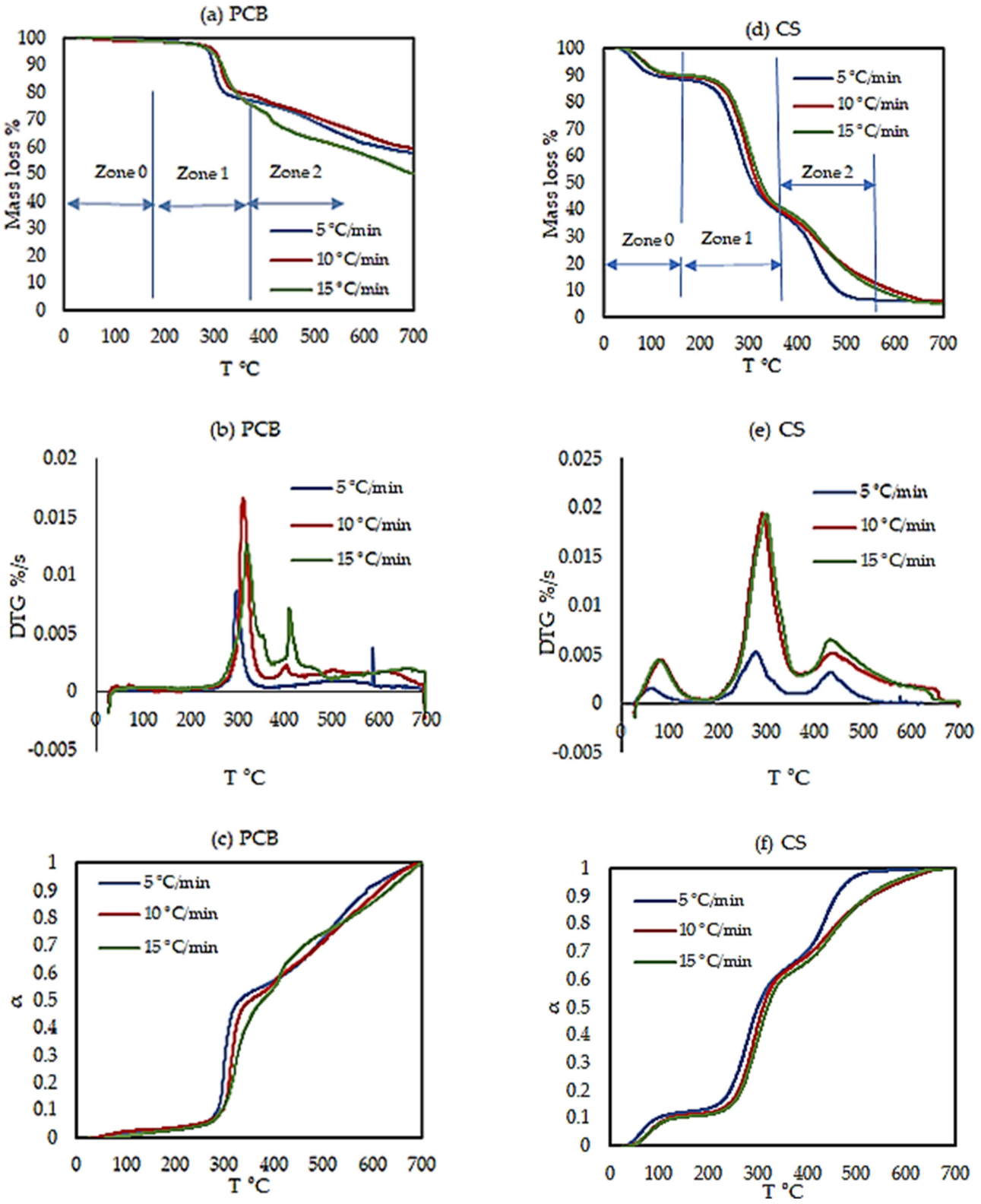

Figure 1. TG-DTG and variation of conversion as a function of temperature plots for the pyrolysis of WPCBs (**a**–**c**) and CS (**d**–**f**).

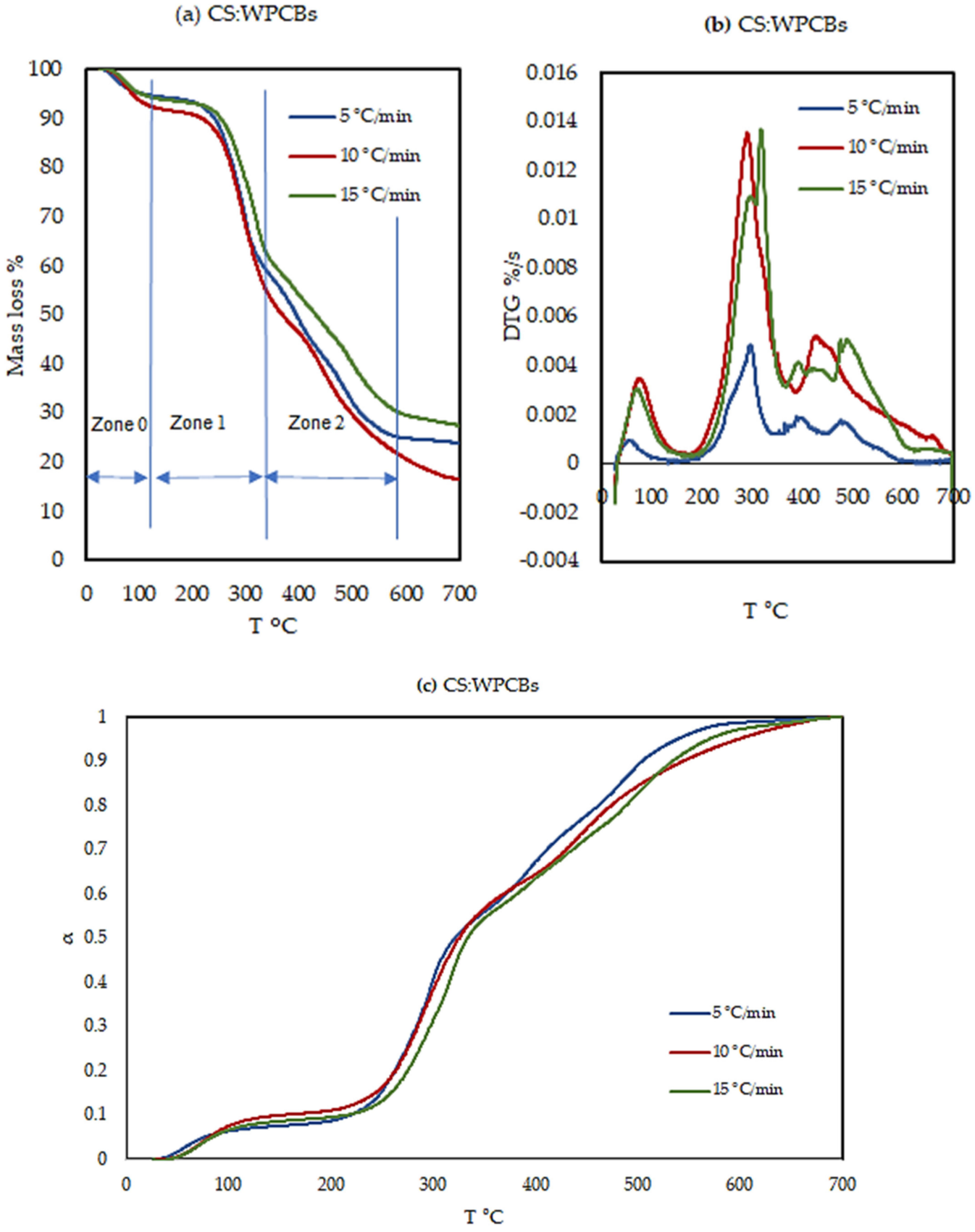

Figure 2. TG-DTG and variation of conversion as a function of temperature plots for the pyrolysis of CS:WPCBs (**a**–**c**).

The main pyrolysis stage of mass loss is termed the region of active pyrolysis. A sharp decline in each TG curve was observed in zones 1 and 2 as shown in Table 4. The degradation profiles of CS:WPCBs samples were initiated at a lower temperature than WPCBs and CS accordingly zones 1 and 2 were defined. Such variation in initial decomposition temperatures is due to the difference in elemental and chemical composition. In these zones, kinetic analysis and mechanism inference were carried out. The appearance of the shoulder in the DTG curve may be due to the degradation of the hemicellulose and lignin in the CS sample and the decomposition of tetra-bromo-bisphenol-A in the WPCBs sample. Whereas, the generated sharp DTG peak relates to the degradation of cellulose and hemicellulose; therefore, a continuous slow degradation may correspond to the slow decomposition of lignin in CS and the mixture. For the WPCBs sample, this is due to the rupture of ether bonds in brominated resin into bisphenol A, propyl alcohol, and tetra-bromo-bisphenol-A. In addition, the epoxy group may rupture, resulting in the release of small molecules. The mass loss in both zones does not have much effect while increasing the heating rate from 5 to 15 K/min. The total weight loss at the end of 700 °C was 42–50, 94–95, and 73–86% for WPCBs, CS, and CS:WPCBs, respectively. The total weight loss over the entire deterioration was larger in samples with more volatile materials and less ash. Tables 4 and 5 show the findings of thermal degradation in an inert atmosphere with mass loss and residue.

Table 4. Mass loss (in %) for first and second zone.

Samples	Heating Rate K/min	First Zone °C				Second Zone °C			
		T_i	T_{max}	T_f	Mass Loss %	T_i	T_{max}	T_f	Mass Loss %
WPCBs	5	180.9	297.1	359.5	22	360.3	494.4	577.1	14
	10	207.6	312.0	369.6	19	370.4	402.2	577.1	13
	15	207.4	319.3	377.3	24	378.0	410.3	577.1	16
CS	5	147.9	279.2	350.7	48	351.4	434.0	571.6	34
	10	172.0	292.3	374.5	50	375.3	436.0	577.1	27
	15	173.5	300.2	376.5	50	377.3	433.1	577.7	30
CS:WPCBs (50:50)	5	121.3	297.3	341.3	36	342.1	387.9	577.4	33
	10	152.2	289.7	371.7	42	372.5	430.3	576.8	28
	15	152.2	317.3	366.1	36	366.8	489.9	577.7	27

Table 5. Mass loss for de-moisturization and char generation.

Sample	Heating Rate K/min	De-Moisturization	Char Generation	Overall Mass Loss %	Residue %
		Mass Loss %	Mass Loss %		
WPCBs	5	1	5	42	58
	10	1.5	6.5	40	60
	15	1.5	8.5	50	50
CS	5	11	1	94	6
	10	11	6	94	6
	15	10	5	95	5
CS:WPCBs (50:50)	5	5	2	76	24
	10	8	6	84	16
	15	6	4	73	27

5.2. FTIR Analysis

FTIR is used to identify various inorganic and organic compounds of the CS:WPCBs pyrolysis oil. The peak in Figure 3 at 3423 cm^{-1} corresponds to the decomposition of hemicellulose and cellulose of CS and O-H stretching of WPCBs. The peaks near 1374 cm^{-1} in oil can be attributed to lignin, mainly due to rings of the type C=C. The peak near 2865 and 2965 cm^{-1} is attributed to C-H stretching of alkane groups and the peak near 1449 cm^{-1} is attributed to C-H bending, indicating the presence of the aldehyde group.

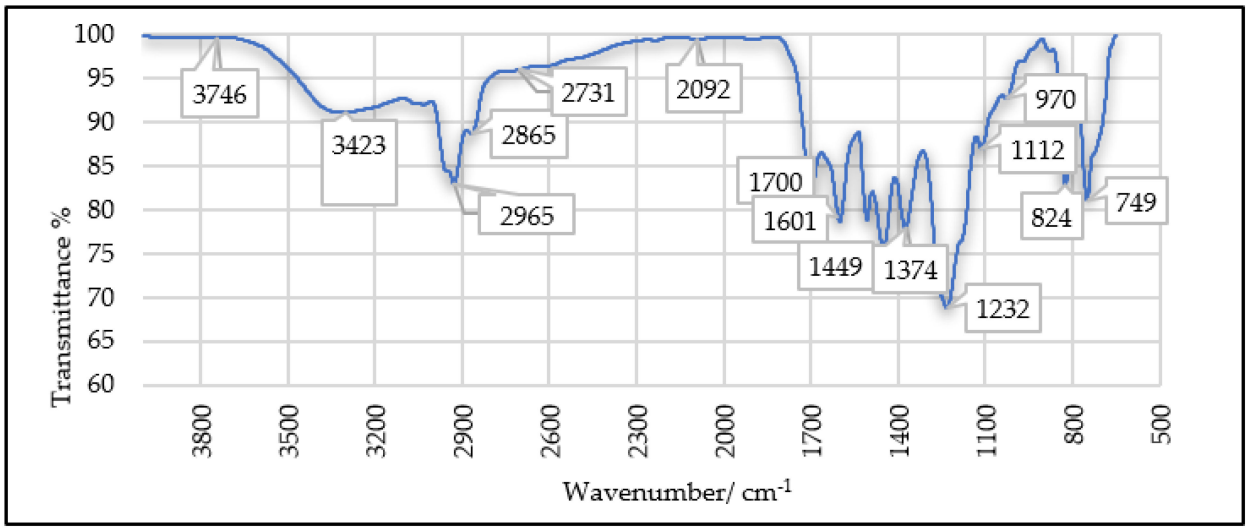

Figure 3. FTIR spectra of pyrolysis oil product of CS:WPCBs.

An absorbance peak with a wavenumber of 749 and 824 cm^{-1} is the indication of C-H bending and ring puckering for the presence of aromatic chemicals in oil. The peak observed around 1601 cm^{-1} may attributed to the C=C and C=O, primarily aldehydes and ketones formed by the dissociation of cellulose and hemicellulose of CS and epoxy resin of WPCBs. The peak at 1232 cm^{-1} can be attributed to the presence of alcohols and phenols, while the peak at 1112 cm^{-1} is associated with C-O-C polysaccharide bond. The peaks at 2731 and 2865 cm^{-1} in the CS:WPCBs pyrolysis oil could be the reason for the presence of HBr indicating that the cleavages of the C(phenyl)–Br have taken place.

5.3. Kinetic Analysis

The results of thermogravimetric analysis were intended to measure the kinetic parameters using model-free methods. Using KAS, FWO, and Starink methods, the apparent activation energy (E_α) and pre-exponential factor (A) was obtained. To determine the kinetic parameters, the value of α ranging from 0.1 to 0.9 during the major thermal decomposition process were chosen, at different heating rates. Furthermore, the results before 0.2 conversion and after 0.9 conversion are having very low values of correlation coefficients and were not reliable. Consequently, an average value was chosen from 0.2 to 0.9 conversion. The FWO, KAS, and Starink plots for different values of conversion of zones 1 and 2 were calculated with Equations (7)–(9) for WPCBs, CS, and CS:WPCBs samples as shown in Figures S1–S3, respectively.

The E_α were obtained from the slopes and compiled in Tables 6–8. The calculated correlation coefficients, R^2, correspond to linear fittings and were higher for all cases except for the WPCBs second zone. This could be as a result of a complex reaction mechanism, implying that the activation energy values are reliable. The reactivity and sensitivity of a reaction rate are also determined by activation energy. A higher value of activation energy indicates the presence of a complex reaction. It can be observed from the results that apparent activation energy for FWO, KAS, and Starink methods are varying significantly for all conversions which shows the presence of a multi-step complicated process in the solid-state matrix. As can be seen in Figures S1–S3 that all the data points are fitting in straight lines at different conversion degrees and are nearly parallel through the isoconversion method that represents the unchanged reaction mechanisms of a single zone of the pyrolysis process in all three samples. The lower the reaction rate is the bigger the space between two consecutive fitting lines. As a result, the scenario suggests that the reaction rate changes as the conversion degree increases. Furthermore, in TG curves, a smaller distance equates to a steeper slope, but in DTG curves, a smaller distance corresponds to a higher reaction rate [39,46].

Table 6. Activation energy (E_α) obtained by model-free methods for WPCBs.

α	First Zone						Second Zone					
	KAS		FWO		Starink		KAS		FWO		Starink	
	E_α (kJ mol^{-1})	R^2	E_α (kJ mol^{-1})	R^2	E_α (kJ mol^{-1})	R^2	E_α (kJ mol^{-1})	R^2	E_α (kJ mol^{-1})	R^2	E_α (kJ mol^{-1})	R^2
0.1	165.98	0.57	166.57	0.59	166.29	0.57	−724.18	0.88	−677.79	0.88	−720.40	0.88
0.2	190.61	0.77	190.21	0.79	190.85	0.77	−202.37	0.95	−181.41	0.94	−200.47	0.95
0.3	168.27	0.97	169.06	0.97	168.60	0.97	−131.06	0.98	−113.41	0.97	−129.41	0.98
0.4	141.89	0.99	144.05	0.99	142.33	0.99	−101.62	0.90	−85.21	0.87	−100.05	0.89
0.5	130.58	0.99	133.37	0.99	131.07	0.99	−97.11	0.83	−80.65	0.79	−95.53	0.83
0.6	120.59	0.99	123.94	0.99	121.12	0.99	−106.57	0.79	−89.36	0.75	−104.93	0.79
0.7	111.12	0.99	115.02	0.99	111.70	0.99	−128.65	0.80	−110.03	0.76	−126.90	0.79
0.8	91.42	0.94	96.42	0.95	92.08	0.94	−242.42	0.76	−217.76	0.74	−240.20	0.76
0.9	88.55	0.92	93.88	0.94	89.24	0.93	−596.35	0.70	−553.80	0.69	−592.79	0.70
Avg.(0.2–0.9)	130.38		133.24		130.87		−200.77		−179.95		−198.78	

Table 7. Activation energy (E_α) obtained by model-free methods for CS.

α	First Zone						Second Zone					
	KAS		FWO		Starink		KAS		FWO		Starink	
	E_α (kJ mol^{-1})	R^2	E_α (kJ mol^{-1})	R^2	E_α (kJ mol^{-1})	R^2	E_α (kJ mol^{-1})	R^2	E_α (kJ mol^{-1})	R^2	E_α (kJ mol^{-1})	R^2
0.1	102.82	0.89	105.90	0.91	103.30	0.9	149.96	0.95	153.04	0.96	150.50	0.96
0.2	118.88	0.93	121.43	0.94	119.33	0.93	195.91	0.96	197.06	0.96	196.33	0.96
0.3	128.57	0.96	130.81	0.96	129.00	0.96	177.49	0.93	179.77	0.94	178.00	0.93
0.4	130.40	0.96	132.7	0.97	130.84	0.96	149.04	0.92	152.92	0.93	149.68	0.93
0.5	139.12	0.96	141.11	0.96	139.54	0.96	135.95	0.93	140.65	0.94	136.64	0.93
0.6	134.81	0.96	137.15	0.97	135.26	0.96	111.55	0.91	117.64	0.92	112.36	0.91
0.7	136.10	0.98	138.50	0.98	136.55	0.98	90.66	0.87	98.00	0.90	91.56	0.88
0.8	141.63	0.99	143.94	0.99	142.09	0.99	80.86	0.87	88.95	0.90	81.83	0.87
0.9	149.72	0.94	151.88	0.95	150.17	0.94	70.26	0.84	79.22	0.88	71.30	0.84
Avg.(0.2–0.9)	134.90		137.19		135.35		126.47		131.78		127.21	

Table 8. Activation energy (E_α) obtained by model-free methods for CS:WPCBs.

α	First Zone						Second Zone					
	KAS		FWO		Starink		KAS		FWO		Starink	
	E_α (kJ mol^{-1})	R^2	E_α (kJ mol^{-1})	R^2	E_α (kJ mol^{-1})	R^2	E_α (kJ mol^{-1})	R^2	E_α (kJ mol^{-1})	R^2	E_α (kJ mol^{-1})	R^2
0.1	131.22	0.99	132.89	0.99	131.60	0.99	90.20	0.64	96.06	0.69	90.95	0.65
0.2	150.59	0.99	151.60	0.99	150.92	0.99	110.74	0.73	115.90	0.76	111.44	0.73
0.3	153.60	0.98	154.67	0.98	153.94	0.98	112.84	0.80	118.16	0.83	113.57	0.81
0.4	161.96	0.98	162.77	0.98	162.29	0.98	120.41	0.93	125.65	0.94	121.14	0.93
0.5	155.81	0.95	157.08	0.95	156.18	0.95	167.41	0.99	170.68	0.99	168.00	0.99
0.6	142.63	0.99	144.68	0.99	143.06	0.99	182.74	0.97	185.58	0.97	183.31	0.97
0.7	135.01	0.96	137.56	0.97	135.49	0.96	212.89	0.96	214.51	0.96	213.37	0.96
0.8	113.92	0.86	117.63	0.88	114.48	0.86	229.06	0.99	230.15	0.99	229.52	0.99
0.9	101.10	0.73	105.67	0.76	101.73	0.73	275.90	0.91	275.06	0.92	276.22	0.91
Avg. (0.2–0.9)	139.33		141.46		139.76		176.50		178.64		177.08	

The kinetic parameters computed using the Starink approach followed the same pattern as those calculated using the KAS method, as shown in Tables 6–8. The FWO approach yields somewhat higher energy values than KAS and Starink, as evidenced by literature [39,46]. Different approximations in equations could be a reason for the discrepancy. The R^2 values derived from the FWO method were higher; therefore, this method was selected for the decomposition mechanism study in the following section.

All three model-free methods are compared in terms of the E_α vs. α (see Figure 4). The ability to recognize multi-step processes and forecast the response "kinetic scheme" over a large temperature range is enabled by understanding E_α vs α. A change in the slope of E_α dependence is usually linked to a change in the overall reaction mechanism's rate-limiting step.

For PCBs, with the FWO method, the calculated E_α for conversion from 0.2 to 0.9 values decreased from 190.21 to 93.88 kJ/mol in the first zone where the average E was 133.25 kJ/mol. In the second zone, it was found fluctuating with an average E = 178.95 kJ/mol, with a positive slope (negative activation energy). This indicates that the rate of reaction decreases with increasing temperature. It can be seen from Table 4 that there is a significant weight loss in this zone so the degradation in this temperature range cannot be neglected.

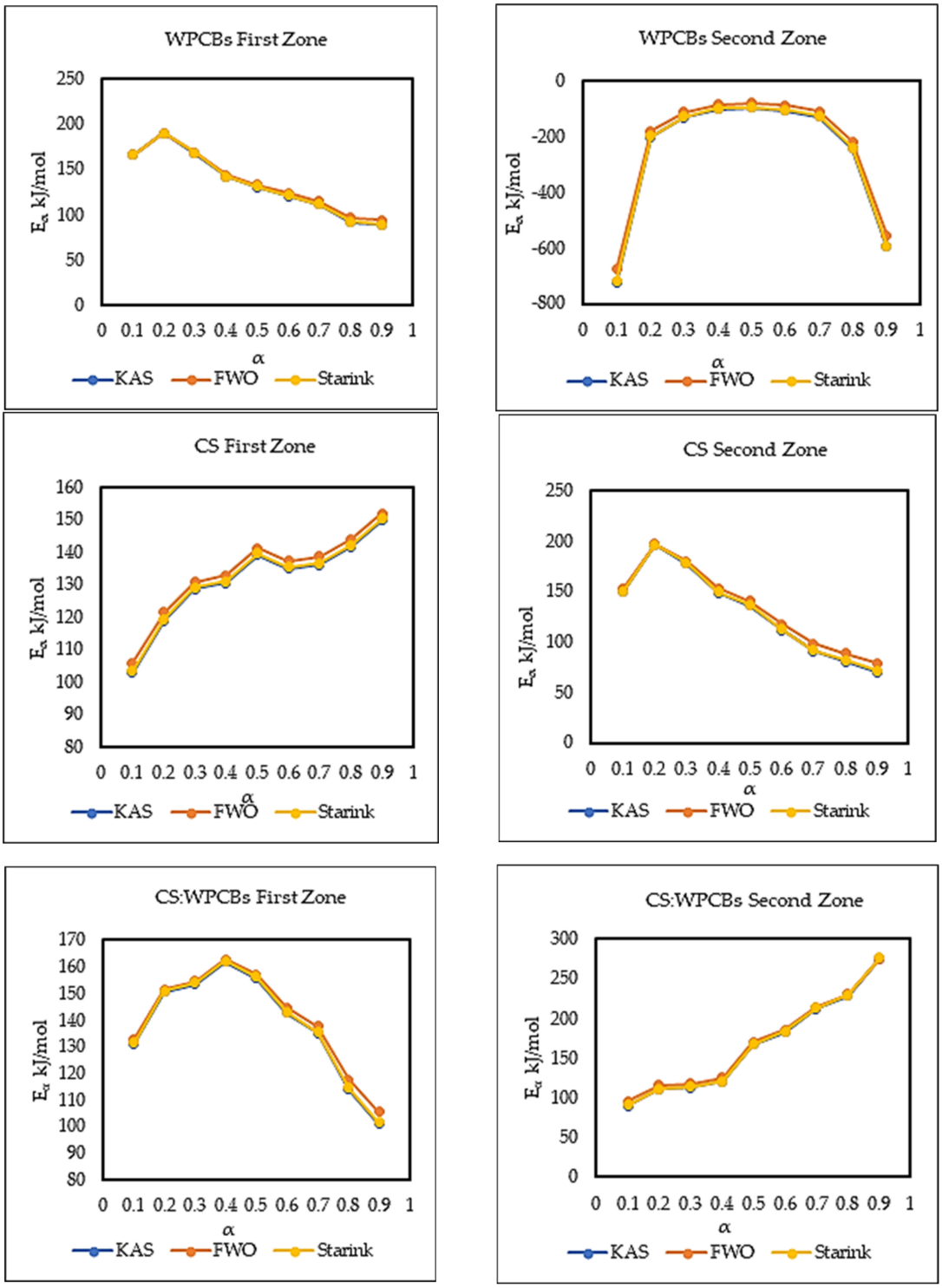

Figure 4. Dependence of activation energy on the conversion (α) for WPCBs, CS, and CS:WPCBs for first and second zone, according to FWO method.

Moreover, in Table 6, the negative activation energy was observed which may take place due to the presence of multi-steps in the process of pyrolysis where the activation energy of one of the steps becomes negative, while the activation energy of the other step remains low. Thus, making the total sum negative, there may be regimes of spontaneous reactions occurring during pyrolysis. According to the researcher [47] who worked on poly (bisphenol A carbonate)-based

polymers originating in waste electric and electronic equipment, the process of heat deterioration is easy to initiate because of the weak link points in the polymer chain.

Random scission becomes the limiting phase of degradation when these weak linkages are depleted, and the activation energy rises to the steady-state value, generally between 210 and 260 kJ/mol. Higher E_α values have also been assigned to the solid carbonaceous char, which protects the polymer from further breakdown and results in a significant amount of solid residue (>20%).

For CS with the FWO method, apparent activation energy is increased from 121.43 to 151.88 kJ/mol (average E = 137.19 kJ/mol) with α ranging from 0.2 to 0.9, it is increased in the second zone up to 0.2 conversion then decreased at the end of the conversion (α = 0.9) to 79.22 kJ/mol (average E = 131.78 kJ/mol). This decrease could be due to the formation of porous chars, which enhanced the diffusion of volatiles.

Table 8 shows the apparent activation energy of CS:WPCBs mixture. Here, prominent effect of WPCBs can be seen in the degradation mechanism. The increasing trend of E_α for α values 0.1–0.4 (132.89–162.77 kJ/mol) may be attributed to the exothermic nature of the decomposition reaction. Whereas, decreases in E_α (162.77–105.67 kJ/mol) with the progressive degree of conversion α from 0.4 to 0.9, are associated with endothermic reaction due to degradation of different components and generation of a small amount of porous char that enhanced the diffusion of volatiles and then reduced the activation energy.

Alkalis metals such as K, Na, Mg, and Ca from reinforcing materials in WPCBs, serve as catalysts, resulting in a decrease in activation energy under high conversion conditions, as illustrated in Figure 5. A vs. α with a high pre-exponential factor means higher conversion. In addition, for second zone the required apparent activation energy is increasing with conversion. As higher E_α indicates a slower reaction, at the second zone it indicates the better thermal stability of the generated char due to the addition of WPCBs in CS.

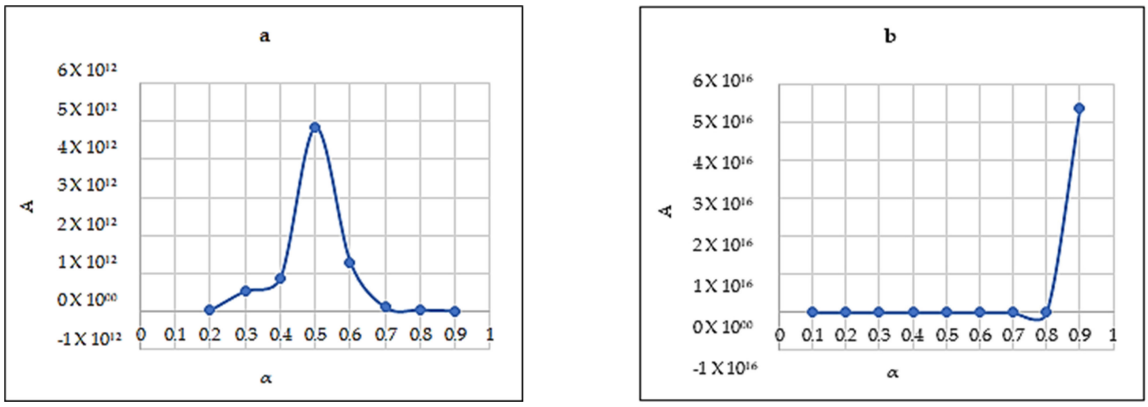

Figure 5. Variation of frequency factor with conversion values for sample CS:WPCBs; (**a**) first zone, and (**b**) second zone.

5.4. Reaction Mechanism

Criado et al. [24,34] proposed a method to determine the geometrical mechanism of the samples at a fixed heating rate, 10 °C/min heating rate was chosen randomly. It is possible to get and overlap the experimental $Z(\alpha)$ values of the master plots using the activation energies estimated with the FWO approach to compare the degradation process that closely approximated the theoretical curves.

Figures 6 and 7 show the master plots and the experimental data obtained by Criado et al. [34]. It is significantly comparable to the m13 mechanism of Table 1, for all three samples except WPCBs second zone. WPCBs second zone shows an odd behavior, so it is difficult to assume its degradation mechanism. The possible reason may be the statistical treatment of the TGA data that can influence the value of the recognized apparent activation energy; other factors may also include the size range of sample particles, and the chemical composition which varies for different parts of WPCBs.

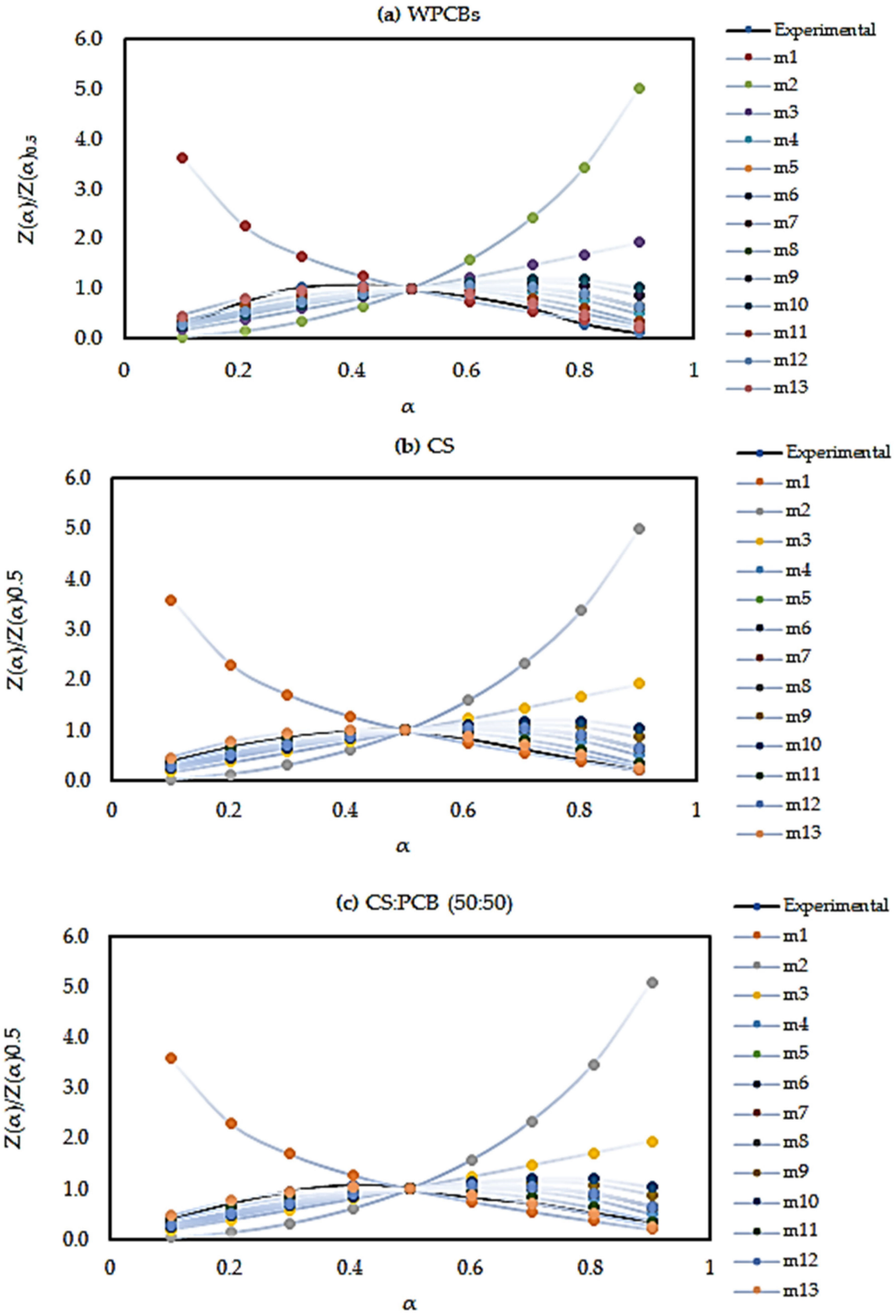

Figure 6. Experimental and theoretical master plots for (**a**) WPCBs, (**b**) CS, and (**c**) CS:WPCBs for first zone with heating rate 10 K/min.

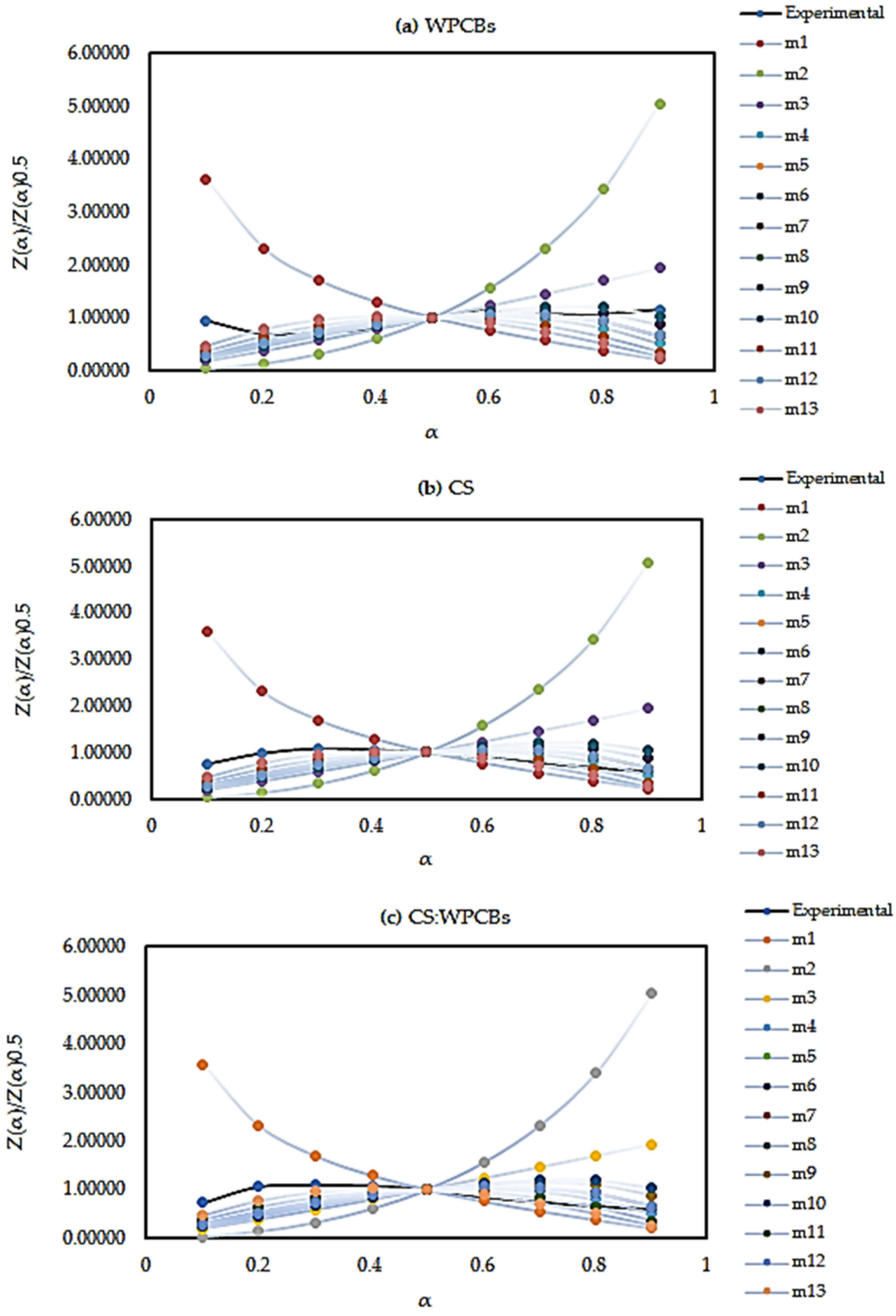

Figure 7. Experimental and Theoretical master plots for (**a**) WPCBs, (**b**) CS and (**c**) CS:WPCBs for second zone with heating rate 10 K/min.

5.5. Kinetic Compensation Effects

Increasing activation energy increases the overall rate of reaction, whereas activation energy must be decreased to accomplish a higher conversion rate. This fact implies that the experimental values of A and E could be correlated. We can fit the experimental data to a rate equation by adjusting the values of A and E in such a compensating manner that their simultaneous change does not affect the overall rate. This correlation is known as a compensation effect and is typically expressed in the following form [31,39],

$$lnA = aE + b \tag{16}$$

where a and b are constants and refer to the compensation coefficients. To validate the kinetic parameters, the m13 mechanism was chosen for calculating the pre-exponential factor as a function of conversion. Substituting $g(\alpha) = ((1-\alpha)^{-2}-1)/2$ and E_α values were determined using the FWO method into Equation (9) will give pre-exponential values. Pre-exponential values were calculated with the FWO method and shown in Table 9 with increasing conversion for CS:WPCBs mixture.

Table 9. Pre-exponential factor from FWO method for CS:WPCBs.

Conversion (α)	**First Zone** ***lnA***	**Second Zone** ***lnA***
0.1	23.00	9.27
0.2	26.99	13.14
0.3	27.49	13.55
0.4	29.21	14.80
0.5	27.87	22.24
0.6	25.20	24.47
0.7	23.86	28.98
0.8	20.20	31.42
0.9	18.66	38.51
Avg (0.2–0.9)	24.94	23.39

An excellent linear relationship, of all three samples, can be found by plotting lnA against E_α, as shown in Figure 8. A linear relationship $lnA = 0.1882E_\alpha - 1.7251$ with $R^2 = 0.9933$ and $lnA = 0.1614E_\alpha - 5.6374$ with $R^2 = 0.9992$ is found for the first and second zones of CS:WPCBs sample, respectively.

The higher values of R^2 indicate that the compensation effect existed between the apparent E_α and lnA during the pyrolysis. The kinetic compensation effect is a valid alternative to demonstrate the interrelationship between the kinetic parameters lnA and E_α. It also shows the impact of experimental conditions on the determination of kinetic parameters.

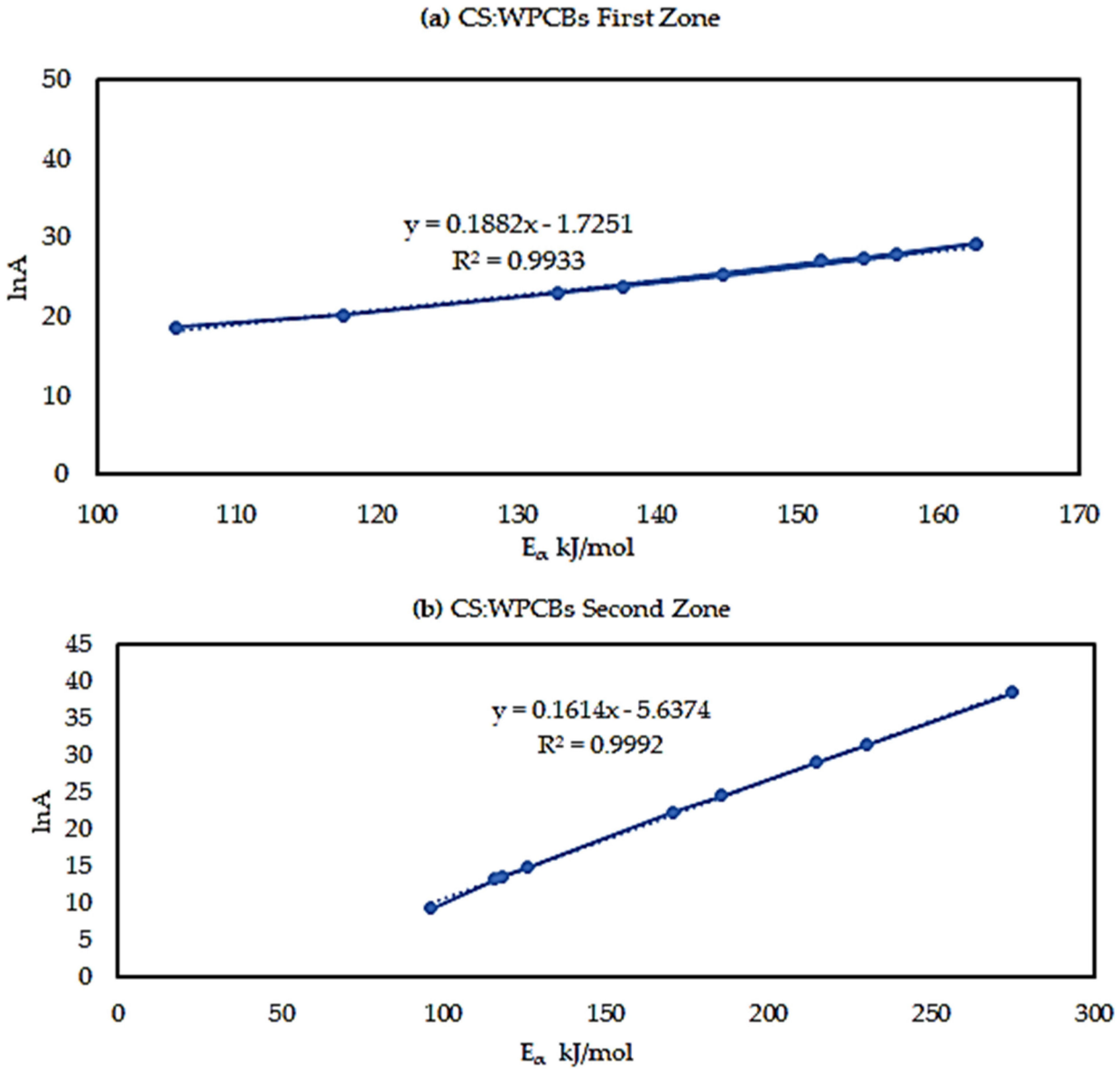

Figure 8. Compensation effect between A and E_α for CS-WPCBs with (**a**) first zone and (**b**) second zone.

6. Conclusions

The thermal decomposition at non-isothermal conditions for WPCBs, CS, and their mixture was investigated. A residue of WPCBs at 700 °C was found to be relatively very high (~60%) compared to 6% for CS and 20% for CS:WPCBs. This high residue of WPCBs is due to the content of high inorganic compounds. The degradation profiles of CS:WPCBs samples were initiated at a lower temperature compared to WPCBs and CS. The total mass loss for CS was not affected by an increased heating rate. However, the mass loss for WPCBs at 15 K/min and for CS:PCB at 10 K/min were significantly high. The weight losses at the final temperature were 42–50 wt%, 94–95 wt%, and 73–76 wt% for WPCBs, CS, and CS:WPCBs, respectively. Total weight loss was higher in samples which had a higher volatile matter and lower ash content.

The E_α from three model-free methods were found to vary significantly. This exhibits the existence of a complex multi-reaction mechanism within the solid matrix, showing that the activation energy is dependent on the conversion mechanism. The kinetic parameters calculated using the Starink method displayed the same trend as those derived from the KAS method. Whereas, the E_α and R^2 values from the FWO method are higher compared

to those of KAS and Starink. FWO method was considered the most reliable method for the reaction mechanism. The average activation energy for all three sample was observed to be between 120 and 200 kJ/mol. Most importantly, PCB second zone has shown a negative value for apparent activation energy E_α. Moreover, the decomposition mechanism was found by the Criado method and it was best described by a third-order reaction, for all three samples. The study of the kinetic compensation effect was used to characterize the dependence of *E* and *lnA*. The results indicated that a compensation effect existed between the apparent activation energy and the pre-exponential factor during the pyrolysis process.

Supplementary Materials: The following supporting information can be downloaded at: https://www.mdpi.com/article/10.3390/pr11010229/s1, Figure S1: Curve fittings to kinetic model proposed by KAS, FWO and Starink for WPCBs 1st (a,b,c) and 2nd (d,e,f) Zone; Figure S2: Curve fittings to kinetic model proposed by KAS, FWO and Starink for CS 1st (a,b,c) and 2nd (d,e,f) Zone; Figure S3: Curve fittings to kinetic model proposed by KAS, FWO and Starink for CS:WPCB 1st (a,b,c) and 2nd (d,e,f) Zone.

Author Contributions: Conceptualization, A.G. and S.G.; methodology, S.B.P.; formal analysis, Z.F.Y.; investigation, S.B.P. and A.G.; resources, F.T. and X.L.; data curation, S.G.; writing—original draft preparation, S.B.P. and S.G.; writing—review and editing, Z.F.Y. and F.T. All authors have read and agreed to the published version of the manuscript.

Funding: The authors declare that no funds, grants, or other support were received during the preparation of this manuscript. Part of the APC for open access publication was funded by Svenska kulturfonden (Swedish Cultural Foundation in Finland), Grant no. SKF-177914, under the E-waste recycling project at Åbo Akademi University.

Data Availability Statement: Not applicable.

Acknowledgments: The authors would like sincerely thanks to Gujarat Environment and Management Institute, Gujarat, India for funding the project (GEMI/726/1001/2017) under Research Scheme-1. The research was carried out under the project. The authors are also grateful to Bharuch Enviro and Infrastructure Ltd., Ankleshwar Gujarat, India for providing analytical facilities.

Conflicts of Interest: The authors declare no conflict of interest.

References

1. Cucchiella, F.; D'Adamo, I.; Lenny Koh, S.C.; Rosa, P. Recycling of WEEEs: An economic assessment of present and future e-waste streams. *Renew. Sustain. Energy Rev.* **2015**, *51*, 263–272. [CrossRef]
2. Abalansa, S.; El Mahrad, B.; Icely, J.; Newton, A. Electronic waste, an environmental problem exported to developing countries: The good, the bad and the ugly. *Sustainability* **2021**, *13*, 5302. [CrossRef]
3. Wang, Z.; Zhang, B.; Guan, D. Take responsibility for electronic-waste disposal. *Nature* **2016**, *536*, 23–25. [CrossRef] [PubMed]
4. Kumar, A.; Holuszko, M.; Espinosa, D.C.R. E-waste: An overview on generation, collection, legislation and recycling practices. *Resour. Conserv. Recycl.* **2017**, *122*, 32–42. [CrossRef]
5. Turaga, R.M.R.; Bhaskar, K.; Sinha, S.; Hinchliffe, D.; Hemkhaus, M.; Arora, R.; Chatterjee, S.; Khetriwal, D.S.; Radulovic, V.; Singhal, P.; et al. E-Waste Management in India: Issues and Strategies. *Vikalpa* **2019**, *44*, 127–162. [CrossRef]
6. Chatterjee, S.D. Electronic Waste and India. Department of Information Technology Electronics Niketan. 2012. Available online: http://meity.gov.in/writereaddata/files/EWaste_Sep11_892011.pdf (accessed on 27 December 2022).
7. Williams, P.T. 6.2 Pyrolysis. In *Waste Treatment and Disposal*; John Wiley & Sons: New York, NY, USA, 2005; pp. 326–337. Available online: http://www.znrfak.ni.ac.rs/serbian/010-studije/oas-3-2/PREDMETI/IIIGODINA/316-KOMUNALNISISTEMIIZIVOTNASREDINA/SEMINARSKIRADOVI/2014/S105-S150.pdf (accessed on 27 December 2022).
8. Williams, P.T. Valorization of printed circuit boards from waste electrical and electronic equipment by pyrolysis. *Waste Biomass Valorization* **2010**, *1*, 107–120. [CrossRef]
9. Rosenberg, C.; Hämeilä, M.; Tornaeus, J.; Säkkinen, K.; Puttonen, K.; Korpi, A.; Kiilunen, M.; Linnainmaa, M.; Hesso, A. Exposure to flame retardants in electronics recycling sites. *Ann. Occup. Hyg.* **2011**, *55*, 658–665.
10. Sepúlveda, A.; Schluep, M.; Renaud, F.G.; Streicher, M.; Kuehr, R.; Hagelüken, C.; Gerecke, A.K. A review of the environmental fate and effects of hazardous substances released from electrical and electronic equipments during recycling: Examples from China and India. *Environ. Impact Assess. Rev.* **2010**, *30*, 28–41. [CrossRef]
11. Salhofer, S. E-waste collection and treatment options: A comparison of approaches in Europe, China and Vietnam. In *Source Separation and Recycling. The Handbook of Environmental Chemistry*; Springer: Cham, Switzerland, 2018; Volume 63, p. 227.

12. Quan, C.; Li, A.; Gao, N. Research on pyrolysis of PCB waste with TG-FTIR and Py-GC/MS. *J. Therm. Anal. Calorim.* **2012**, *110*, 1463–1470. [CrossRef]
13. Kim, Y.; Kim, S.; Lee, J.; Park, Y. Pyrolysis Reaction Pathways of Waste Epoxy-Printed Circuit Board. *Environ. Eng. Sci.* **2013**, *30*, 706–712. [CrossRef]
14. Ankit; Saha, L.; Kumar, V.; Tiwari, J.; Sweta; Rawat, S.; Singh, J.; Bauddh, K. Electronic waste and their leachates impact on human health and environment: Global ecological threat and management. *Environ. Technol. Innov.* **2021**, *24*, 102049. [CrossRef]
15. Dhaundiyal, A.; Singh, S.B.; Hanon, M.M.; Rawat, R. Determination of Kinetic Parameters for the Thermal Decomposition of Parthenium hysterophorus. *Environ. Clim. Technol.* **2018**, *22*, 5–21. [CrossRef]
16. Diaz, F.; Flerus, B.; Nagraj, S.; Bokelmann, K.; Stauber, R.; Friedrich, B. Comparative Analysis About Degradation Mechanisms of Printed Circuit Boards (PCBs) in Slow and Fast Pyrolysis: The Influence of Heating Speed. *J. Sustain. Metall.* **2018**, *4*, 205–221. [CrossRef]
17. Abdou, T.R.; Botelho, A.B., Jr.; Espinosa, D.C.R.; Tenório, J.A.S. Recycling of polymeric composites from industrial waste by pyrolysis: Deep evaluation for carbon fibers reuse. *Waste Manag.* **2021**, *120*, 1–9. [CrossRef] [PubMed]
18. Liu, W.J.; Tian, K.; Jiang, H.; Zhang, X.S.; Yang, G.X. Preparation of liquid chemical feedstocks by co-pyrolysis of electronic waste and biomass without formation of polybrominated dibenzo-p-dioxins. *Bioresour. Technol.* **2013**, *128*, 1–7. [CrossRef]
19. Abnisa, F.; Wan Daud, W.M.A. A review on co-pyrolysis of biomass: An optional technique to obtain a high-grade pyrolysis oil. *Energy Convers. Manag.* **2014**, *87*, 71–85. [CrossRef]
20. Radojević, M.; Janković, B.; Jovanović, V.; Stojiljković, D.; Manić, N. Comparative pyrolysis kinetics of various biomasses based on model-free and DAEM approaches improved with numerical optimization procedure. *PLoS ONE* **2018**, *13*, e0206657. [CrossRef]
21. Shen, Y.; Chen, X.; Ge, X.; Chen, M. Thermochemical treatment of non-metallic residues from waste printed circuit board: Pyrolysis vs. combustion. *J. Clean. Prod.* **2018**, *176*, 1045–1053. [CrossRef]
22. Conesa, J.A.; Soler, A. Decomposition kinetics of materials combining biomass and electronic waste. *J. Therm. Anal. Calorim.* **2017**, *128*, 225–233. [CrossRef]
23. Holba, P. Temperature dependence of activation energy of endothermic processes and related imperfections of non-isothermal kinetic evaluations. *J. Therm. Anal. Calorim.* **2017**, *129*, 609–614. [CrossRef]
24. Criado, J.M.; Pérez-Maqueda, L.A.; Sánchez-Jiménez, P.E. Dependence of the preexponential factor on temperature: Errors in the activation energies calculated by assuming that A is constant. *J. Therm. Anal. Calorim.* **2005**, *82*, 671–675. [CrossRef]
25. Vyazovkin, S. Kinetic concepts of thermally stimulated reactions in solids: A view from a historical perspective. *Int. Rev. Phys. Chem.* **2000**, *19*, 45–60. [CrossRef]
26. Vyazovkin, S. A time to search: Finding the meaning of variable activation energy. *Phys. Chem. Chem. Phys.* **2016**, *18*, 18643–18656. [CrossRef] [PubMed]
27. Šimon, P. Isoconversional methods: Fundamentals, meaning and application. *J. Therm. Anal. Calorim.* **2004**, *76*, 123–132. [CrossRef]
28. Guida, M.Y.; Hannioui, A. Evaluation of Reliability of Coats-Redfern and Criado Methods for Kinetics Analysis of Olive Mill Solid Waste and Olive Mill Wastewater. *Int. J. Sci. Eng. Res.* **2016**, *7*, 193–203.
29. Hammani, H. Investigation on the Pyrolysiskinetics and Mechanism of Date Stone Using Thermogravimetric Analysis. *Eng. Technol. J.* **2018**, *3*, 366–375. [CrossRef]
30. Starink, M.J. The determination of activation energy from linear heating rate experiments: A comparison of the accuracy of isoconversion methods. *Thermochim. Acta* **2003**, *404*, 163–176. [CrossRef]
31. Hu, Y.; Wang, Z.; Cheng, X.; Ma, C. Non-isothermal TGA study on the combustion reaction kinetics and mechanism of low-rank coal char. *RSC Adv.* **2018**, *8*, 22909–22916. [CrossRef] [PubMed]
32. Koga, N. Ozawa's kinetic method for analyzing thermoanalytical curves: History and theoretical fundamentals. *J. Therm. Anal. Calorim.* **2013**, *113*, 1527–1541. [CrossRef]
33. Venkatesh, M.; Ravi, P.; Tewari, S.P. Isoconversional kinetic analysis of decomposition of nitroimidazoles: Friedman method vs Flynn-Wall-Ozawa method. *J. Phys. Chem. A* **2013**, *117*, 10162–10169. [CrossRef]
34. Criado, J.M.; Málek, J.; Ortega, A. Applicability of the master plots in kinetic analysis of non-isothermal data. *Thermochim. Acta* **1989**, *147*, 377–385. [CrossRef]
35. Pistor, V.; Ornaghi, F.G.; Ornaghi, H.L.; Zattera, A.J. Degradation kinetic of epoxy nanocomposites containing different percentage of epoxycyclohexyl-POSS. *Polym. Compos.* **2012**, *33*, 1224–1232. [CrossRef]
36. Aboulkas, A.; El Harfi, K. Study of the kinetics and mechanisms of thermal decomposition of Moroccan Tarfaya oil shale and its kerogen. *Oil Shale* **2008**, *25*, 426–443. [CrossRef]
37. Kissinger, R. Reaction Kinetics in Differential Thermal Analysis. *Anal. Chem.* **1957**, *303*, 1702–1706. [CrossRef]
38. Guida, M.Y.; Bouaik, H.; El Mouden, L.; Moubarik, A.; Aboulkas, A.; El Harfi, K.; Hannioui, A. Utilization of Starink Approach and Avrami Theory to Evaluate the Kinetic Parameters of the Pyrolysis of Olive Mill Solid Waste and Olive Mill Wastewater. *J. Adv. Chem. Eng.* **2017**, *7*, 1–8.
39. Yao, Z.; Xiong, J.; Yu, S.; Su, W.; Wu, W.; Tang, J.; Wu, D. Kinetic study on the slow pyrolysis of nonmetal fraction of waste printed circuit boards (NMF-WPCBs). *Waste Manag. Res.* **2020**, *38*, 903–910. [CrossRef] [PubMed]
40. Prajapati, S.B.; Gautam, A.; Gautam, S. Debromination and improved phenol content in fuel oil generated from co-pyrolysis of non-metallic PCB and biomass. *Biomass Convers. Biorefin.* **2022**, 1–17. [CrossRef]

41. Bizzo, W.A.; Figueiredo, R.A.; De Andrade, V.F. Characterization of printed circuit boards for metal and energy recovery after milling and mechanical separation. *Materials* **2014**, *7*, 4555–4566. [CrossRef] [PubMed]
42. Barontini, F.; Marsanich, K.; Petarca, L.; Cozzani, V. Thermal degradation and decomposition products of electronic boards containing BFRs. *Ind. Eng. Chem. Res.* **2005**, *44*, 4186–4199. [CrossRef]
43. Barontini, F.; Marsanich, K.; Petarca, L.; Cozzani, V. The Thermal Degradation Process of Tetrabromobisphenol A. *Ind. Eng. Chem. Res.* **2004**, *43*, 1952–1961. [CrossRef]
44. Grause, G.; Furusawa, M.; Okuwaki, A.; Yoshioka, T. Pyrolysis of tetrabromobisphenol-A containing paper laminated printed circuit boards. *Chemosphere* **2008**, *71*, 872–878. [CrossRef] [PubMed]
45. Luda, M.P.; Balabanovich, A.I.; Zanetti, M.; Guaratto, D. Thermal decomposition of fire retardant brominated epoxy resins cured with different nitrogen containing hardeners. *Polym. Degrad. Stab.* **2007**, *92*, 1088–1100. [CrossRef]
46. Chen, D.; Shuang, E.; Liu, L. Analysis of pyrolysis characteristics and kinetics of sweet sorghum bagasse and cotton stalk. *J. Therm. Anal. Calorim.* **2018**, *131*, 1899–1909. [CrossRef]
47. Siddiqui, M.N.; Redhwi, H.H.; Antonakou, E.V.; Achilias, D.S. Pyrolysis mechanism and thermal degradation kinetics of poly(bisphenol A carbonate)-based polymers originating in waste electric and electronic equipment. *J. Anal. Appl. Pyrolysis* **2018**, *132*, 123–133. [CrossRef]